POÇOS DE CALDAS PROJECT

NAGRA NTB 90-32
SKB TR 90-23
UK DOE WR 90-054

Poços de Caldas Report No. 14

Geochemical modelling of water-rock interactions at the Osamu Utsumi mine and Morro do Ferro analogue study sites, Poços de Caldas, Brazil

An international project with the participation of Brazil, Sweden (SKB), Switzerland (NAGRA), United Kingdom (UK DOE) and USA (US DOE). The project is managed by SKB, Swedish Nuclear Fuel and Waste Management Co.

POÇOS DE CALDAS PROJECT

NAGRA NTB 90-32
SKB TR 90-23
UK DOE WR 90-054

Poços de Caldas Report No. 14

Geochemical modelling of water-rock interactions at the Osamu Utsumi mine and Morro do Ferro analogue study sites, Poços de Caldas, Brazil

An international project with the participation of Brazil, Sweden (SKB), Switzerland (NAGRA), United Kingdom (UK DOE) and USA (US DOE). The project is managed by SKB, Swedish Nuclear Fuel and Waste Management Co.

Geochemical modelling of water-rock interactions at the Osamu Utsumi mine and Morro do Ferro analogue study sites, Poços de Caldas, Brazil.

D.K. NORDSTROM[1], I. PUIGDOMÈNECH[2] and R.H. McNUTT[3].

[1]U.S. Geological Survey, Menlo Park, CA. 94025 (U.S.A.).

[2]Studsvik AB, S-611 82 Nyköping (Sweden).

[3]Department of Geology, McMaster University, Ontario, N2L 3G1 (Canada).

Abstract

Geochemical processes involving water-rock-gas interactions have been modelled using groundwater compositions, mineralogical data, ion plots and computations of speciation, non-thermodynamic mass balance and thermodynamic mass transfer for two natural analogue sites near Poços de Caldas, Brazil: the Osamu Utsumi mine and Morro do Ferro. The main rock type is an alkaline igneous complex composed of volcanic and sub-volcanic phonolites that have been hydrothermally altered and highly weathered. This altered rock mass grades from a laterite at the surface to a saprolite and finally to unweathered, hydrothermally altered bedrock at depth. The mine site contains high concentrations of uranium and Morro do Ferro contains high concentrations of thorium and rare-earths. The reaction models can reproduce the water chemistry and mineral occurrences and they were validated by predicting the masses of minerals precipitated and the pH of the final water. The model computations can also reproduce the pH and iron concentrations of the water samples during CO_2 degassing and iron(II) oxidation from exposure to air. The results from the geochemical reaction models reveal that the dominant processes are production of CO_2 in the soil zone through aerobic decay of organic matter, dissolution of fluorite, calcite, K-feldspar, albite and manganese oxides, oxidation of pyrite and sphalerite and precipitation of ferric oxides, silica and kaolinite. Recharge waters are undersaturated with respect to barite and discharging waters and deeper groundwaters are saturated to supersaturated with respect to barite, demonstrating a strong equilibrium solubility control. Strontium isotope data demonstrate that sources other than calcium-bearing minerals are required to account for the dissolved strontium in the groundwaters. These may include K-feldspar, smectite-chlorite mixed-layer clays and goyazite.

Zusammenfassung

Für zwei Forschungsgelände zum Studium natürlicher Analoga in der Nähe von Poços de Caldas, Brasilien (Osamu Utsumi Mine und Morro do Ferro), wurden geochemische Vorgänge, die Wasser/Gestein/Gas-Wechselwirkungen betreffen, modelliert anhand von Grundwasserzusammensetzungen, mineralogischen Daten, Ionenkorrelationen, Speziationsrechnungen, Ionenbilanzen und Lösungsgleichgewichten. Die Hauptgesteinsarten sind alkalisches Eruptivgestein, das aus hydrothermal veränderten und stark verwitterten, vulkanischen und subvulkanischen Phonoliten besteht. Diese veränderte Gesteinsmasse variiert von Lateriten an der Oberfläche zu Saproliten und schlussendlich zu unverwittertem, hydrothermal verändertem Grundgestein in der Tiefe. Die Mine enthält hohe Konzentrationen an Uran, und Morro do Ferro hat hohe Konzentrationen an Thorium und Seltenen Erden. Die Reaktionsmodelle können die Wasserchemie und Mineralvorkommen wiedergeben und wurden durch Vorhersagen über ausgefällte Mengen von Mineralien und den pH-Wert des Endwassers bestätigt. Die Modellberechnungen können auch den pH-Wert und Eisengehalt der Wasserproben während der CO_2-Entgasung und der Eisen(II)oxydation bei Luftzutritt wiedergeben. Die Resultate der geochemischen Reaktionsmodelle zeigen, dass die vorherrschenden Vorgänge folgende sind: Erzeugung von CO_2 in der Bodenschicht durch Oxydation organischer Stoffe; Auflösung von Fluorit, Calcit, K-Feldspat, Albit, Manganoxyden; Oxydation von Pyrit und Sphalerit; Ausfällung von Eisenoxyden, Kieselsäure und Kaolinit. Frisch gespeicherte Grundwässer sind untersättigt bezüglich Baryt, während abfliessende Wässer und tiefere Grundwässer an Baryt gesättigt bis übersättigt sind, was die bestimmende Wirkung der Gleichgewichts-Löslichkeit zeigt. Strontium-Isotopen-Daten zeigen, dass andere Quellen als calciumhaltige Mineralien benötigt werden, um das gelöste Strontium der Grundwässer zu erklären. Diese könnten K-Feldspat, Smectit-Chlorit-Mischschichttone und Goyazit einschliessen.

Résumé

On a modélisé des processus géochimiques relatifs aux interactions eau-roche-gaz en utilisant la composition des eaux souterraines, des données minéralogiques, des balances ioniques et des calculs de spéciations, de bilans de masse non-thermodynamiques et de transferts de masse thermodynamiques pour deux sites d'étude d'analogies naturelles proches de Poços de Caldas au Brésil: la mine d'Osamu Utsumi et Morro do Ferro. Le principal type de roches est un complexe alcalin igné, composé de phonolites volcaniques et subvolcaniques altérées hydrothermalement et fortement décomposées par les agents atmosphériques. Cette masse de roche altérée passe d'une latérite en surface à une saprolite et finalement en profondeur à une roche en place non effritée, altérée hydrothermalement. Le site de la mine contient de fortes concentrations d'uranium alors que Morro do Ferro présente d'importantes concentrations de thorium et de terres rares. Les modèles de réactions peuvent reproduire la chimie des eaux et l'occurence de minéraux; ils ont été validés en prédisant la masse des minéraux précipités et le pH de l'eau résultante. Les calculs réalisés à l'aide des modèles peuvent également reproduire le pH et les teneurs en fer des échantillons d'eau lors du dégazage de CO_2 et l'oxydation du fer (II) par exposition à l'air. Les résultats des modèles de réactions géochimiques révèlent que les processus dominants sont la production de CO_2 dans le sol par décomposition aérobique de matières organiques, la dissolution de fluorite, de calcite, de feldspath potassique, d'albite, d'oxydes de manganèse, l'oxydation de pyrite et de sphalérite et la précipitation d'oxydes ferriques, de silice et de kaolinite. Les eaux d'infiltration sont sous-saturées en barite et les eaux résurgentes ainsi que les eaux souterraines profondes sont saturées ou sursaturées en barite, démontrant un important mécanisme de contrôle de l'équilibre des solubilités. Des données isotopiques pour le strontium démontrent que des sources autres que les minéraux calciques sont nécessaires pour expliquer la quantité de strontium dissous dans les eaux souterraines, comme les felspaths potassiques, les argiles à couches alternées smectite-chlorite et les goyazites.

Preface

The Poços de Caldas Project was designed to study processes occurring in a natural environment which contains many features of relevance for the safety assessment of radioactive waste disposal. The study area, in the State of Minas Gerais, Brazil, is a region of high natural radioactivity associated with volcanic rocks, geothermal springs and uranium ore deposits. It contains two sites of particular interest on which the project work was focussed: the Osamu Utsumi uranium mine and the Morro do Ferro thorium/rare-earth ore body. The first site is notable in particular for the prominent redox fronts contained in the rock, while Morro do Ferro was already well-known as one of the most naturally radioactive locations on the surface of the Earth, owing to the high thorium ore grade and the shallow, localised nature of the deposit.

The features displayed by these two sites presented the opportunity to study a number of issues of concern in repository performance assessment. The four objectives set after the first-year feasibility study were:

1. Testing of equilibrium thermodynamic codes and their associated databases used to evaluate rock/water interactions and solubility/speciation of elements.
2. Determining interactions of natural groundwater colloids with radionuclides and mineral surfaces, with emphasis on their role in radionuclide transport processes.
3. Producing a model of the evolution and movement of redox fronts, with the additional aim of understanding long-term, large-scale movements of trace elements and rare-earths over the front (including, if possible, natural Pu and Tc).
4. Modelling migration of rare-earths (REE) and U-Th series radionuclides during hydrothermal activity similar to that anticipated in the very near-field of some spent-fuel repositories.

The project ran for three and a half years from June 1986 until December 1989 under the joint sponsorship of SKB (Sweden), NAGRA (Switzerland), the Department of the Environment (UK) and the Department of Energy (USA), with considerable support from a number of organisations in Brazil, notably Nuclebrás (now Urânio do Brasil). The first-year feasibility study was followed by two and a half years of data collection and interpretation, focussed on the four objectives above.

This report is one of a series of 15, summarising the technical aspects of the work and presenting the background data. A complete list of reports is given below. Those in series A present data and interpretations of the sites, while those in series B present the results of modelling the data with performance assessment objectives in mind. The main findings of the project are presented in a separate summary (no. 15).

This report presents a geochemical interpretation of the groundwaters at both sites using ion plots, mineralogical and isotopic data and aqueous geochemical models. This interpretation (objective 1) sets the background for further modelling work on trace element chemistry, redox front chemistry, colloid chemistry and microbiology.

Poços de Caldas Project Report Series

Series A: Data, Descriptive, Interpretation

Report No.	Topic	Authors (Lead in Capitals)
1.	The regional geology, mineralogy and geochemistry of the Poços de Caldas alkaline caldera complex, Minas Gerais, Brazil.	SCHORSCHER, Shea.
2.	Mineralogy, petrology and geochemistry of the Poços de Caldas analogue study sites, Minas Gerais, Brazil. I: Osamu Utsumi uranium mine.	WABER, Schorscher, Peters.
3.	Mineralogy, petrology and geochemistry of the Poços de Caldas analogue study sites, Minas Gerais, Brazil. II: Morro do Ferro.	WABER.
4.	Isotopic geochemical characterization of selected nepheline syenites and phonolites from the Poços de Caldas alkaline complex, Minas Gerais, Brazil.	SHEA.
5.	Geomorphological and hydrogeological features of the Poços de Caldas caldera and the Osamu Utsumi mine and Morro do Ferro analogue study sites, Brazil.	HOLMES, Pitty, Noy.
6.	Chemical and isotopic composition of groundwaters and their seasonal variability at the Osamu Utsumi and Morro do Ferro analogue study sites, Poços de Caldas, Brazil.	NORDSTROM, Smellie, Wolf.
7.	Natural radionuclide and stable element studies of rock samples from the Osamu Utsumi mine and Morro do Ferro analogue study sites, Poços de Caldas, Brazil.	MacKENZIE, Scott, Linsalata, Miekeley, Osmond, Curtis.
8.	Natural series radionuclide and rare-earth element geochemistry of waters from the Osamu Utsumi mine and Morro do Ferro analogue study sites, Poços de Caldas, Brazil.	MIEKELEY, Coutinho de Jesus, Porto da Silveira, Linsalata, Morse, Osmond.

Contents

1. Introduction

Characterisation and interpretation of groundwater geochemistry is an important component of the performance assessment of subsurface radioactive waste disposal. Transport of radionuclides in groundwaters is affected by adsorption and desorption processes and dissolution and precipitation reactions. The effectiveness of these processes is being studied not only in the laboratory but also in the field as part of natural analogue studies aimed at characterising the mobility of naturally occurring radionuclides. The first step in understanding and characterising these processes, either in an analogue study or during a site investigation, is to construct a model describing the rock-water reactions controlling the basic hydrochemistry of the groundwater system. In the current study, this forms a basis for subsequent modelling of trace element behaviour (Bruno *et al.*, this report series; Rep. 11) and the development of weathering and redox fronts (McKinley (Ed.), this report series; Rep. 12).

The two sites considered in the current investigations (Morro do Ferro and the Osamu Utsumi mine) have a similar geological history (see Waber *et al.*; Waber, this report series; Reps. 2 and 3) and the groundwater chemistry is also comparable, except where mining activities have changed the groundwater flow patterns at the mine site and increased the production of acid mine waters as a result of pyrite oxidation.

This report presents a geochemical interpretation of the groundwaters at both sites using ion plots, mineralogical and isotopic data and aqueous geochemical models. This interpretation sets the background for further modelling work on trace element chemistry, redox front chemistry, colloid chemistry and microbiology.

2. Field sites

2.1. Osamu Utsumi mine

The Osamu Utsumi mine is an open pit uranium mine located in the central plateau region of Brazil, near Poços de Caldas, Minas Gerais (Fig. 1). The mine is part of a large caldera composed mainly of volcanic and sub-volcanic phonolites that formed about 80 million years ago. Shortly after the formation of the alkaline igneous complex, hydrothermal fluids altered the mine area and enriched the bedrock in uranium, rare-earths, potassium and zinc. Following hydrothermal alteration the site was uplifted and exposed to about 75 million years of weathering. Details of the geochronology,

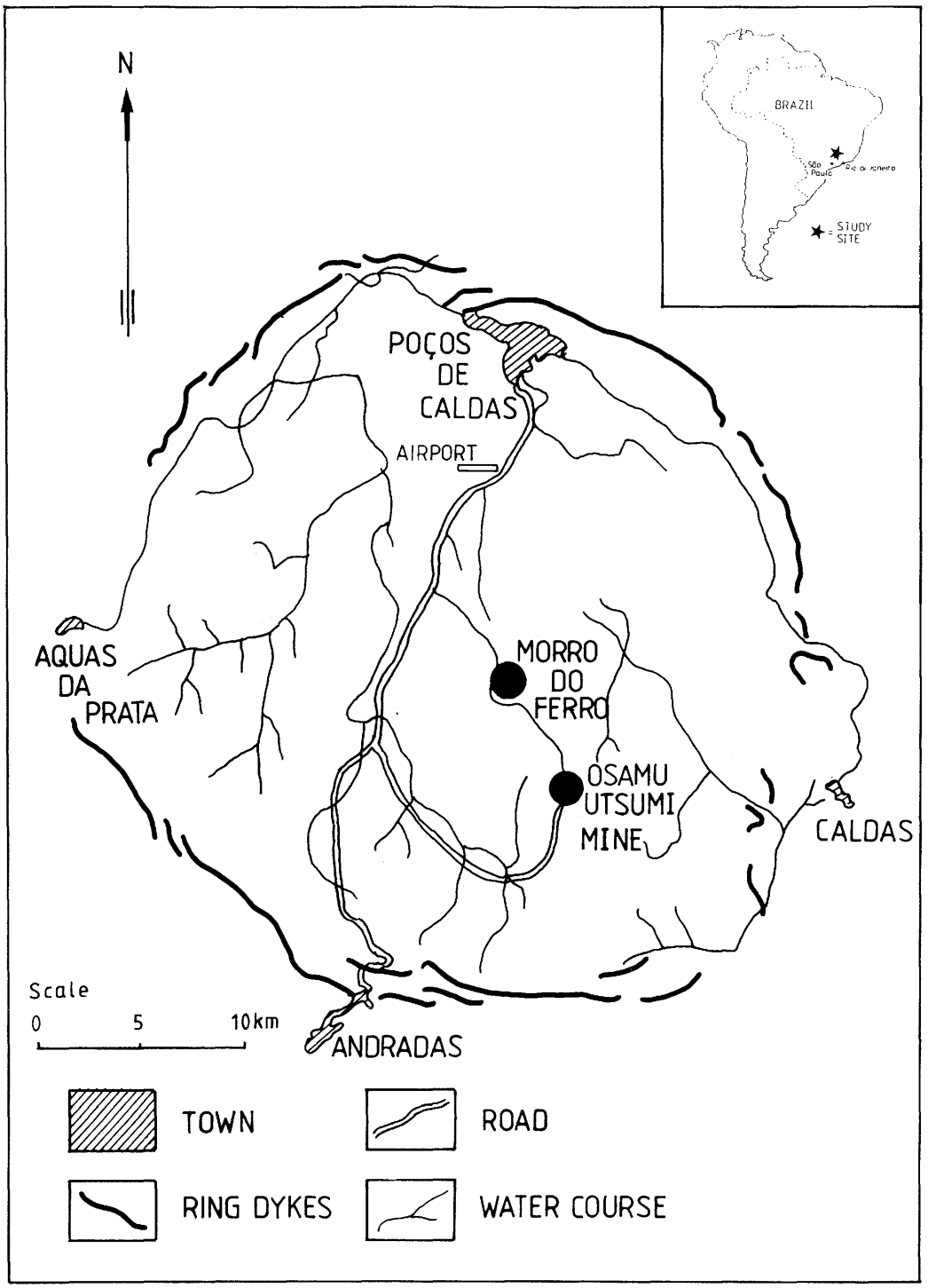

Figure 1. Location of the Osamu Utsumi mine and Morro do Ferro natural analogue study sites.

petrology and mineralogy can be found in Schorscher and Shea, Waber *et al.*, Waber and Shea (this report series; Reps. 1-4).

This site has been open pit-mined to a depth of about 100 m, exposing a well-defined redox front consisting of pervasive iron oxyhydroxides in the upper part and pyrites in the lower part. Mineralisation includes pitchblende, pyrite, sphalerite, fluorite, barite and molybdenite. K-feldspar and nepheline tend to dominate the primary mineralogy. The weathered zone consists of gibbsite and kaolinite near the surface grading into an illite-kaolinite-smectite-chlorite assemblage at depth. Minor or accessory minerals include alunite, florencite, jarosite, pyrophyllite, apatite and zircon.

Locations of boreholes are shown on the mine map in Figure 2 and in the cross-section of Figure 3. Water samples were collected by pumping up through nylon tubing from packed-off sections of the boreholes as shown in Figure 3. Probable directions of groundwater flow are designated by the arrows. Water samples were also collected from an old mine shaft, some piezometer holes and some ponded surface water.

2.2. Morro do Ferro

The hill named Morro do Ferro has a highly weathered bedrock into which 2 pairs of boreholes have been drilled (Fig. 4). Boreholes MF10 and MF11 were drilled into the recharge zone of the hill and their mineralogy at depth (carbonates, jacobsite, magnetite, apatite) suggests the primary rock may have been a carbonatite. The weathered rock consists of kaolinite, illite and gibbsite, with minor magnetite, florencite, jacobsite, psilomelane and lithio philite.

Boreholes MF12 and MF13 were drilled into the discharge zone which is composed of typical altered phonolite as seen at the Osamu Utsumi mine.

3. Sampling and analytical protocols

The sampling and analytical protocols have been described in detail in Nordstrom *et al.* (this report series; Rep. 6) and will therefore only be briefly mentioned here.

Two sampling programmes were carried out:

1) Approximately year-round twice-weekly sampling for selected constituents (Fe(II), Fe(tot), pH, Eh, SO_4, HCO_3, U, F). Later in the programme Na, K, DO (dissolved oxygen) and COD (chemical oxygen demand) were included.

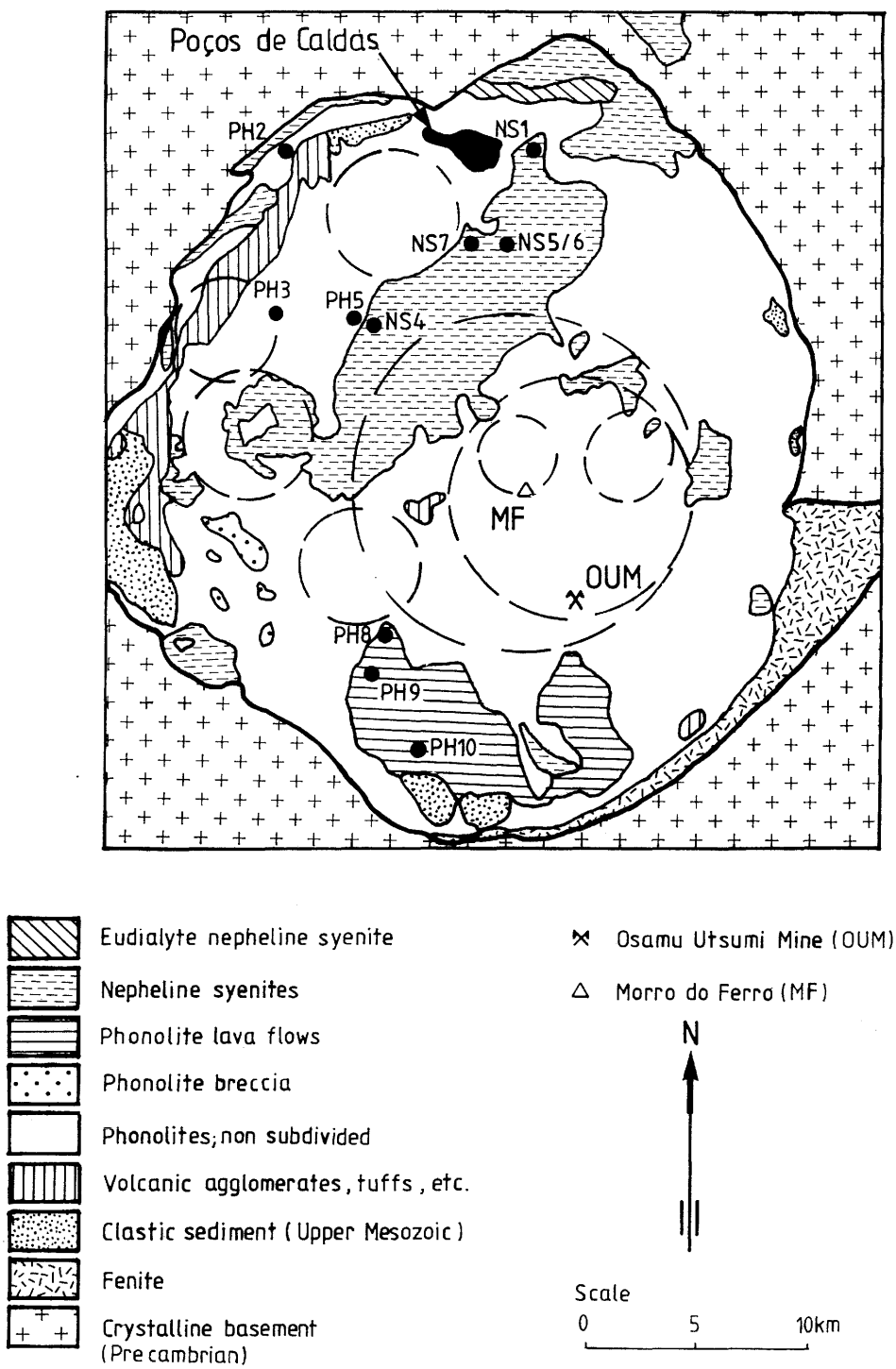

Figure 2. A simplified geologic map (after Ellert et al., 1959, and Almeida Filho and Paradella, 1977) of the Poços de Caldas caldera. Circular features within the caldera are mainly derived from topographic analysis.

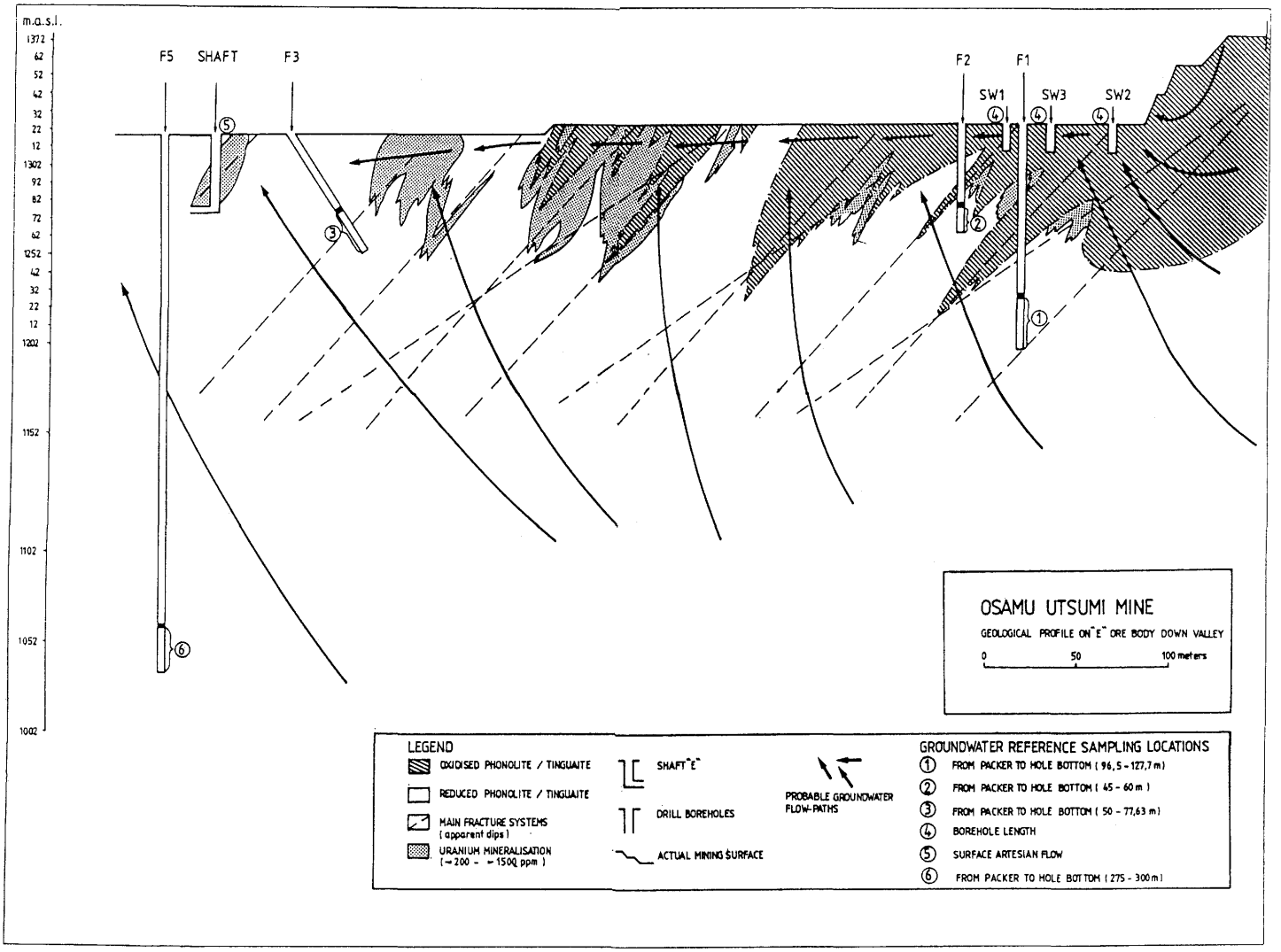

Figure 3. Cross-section of Osamu Utsumi mine showing borehole locations, redox fronts, mineralised zones, groundwater reference sampling locations and general direction of groundwater flow.

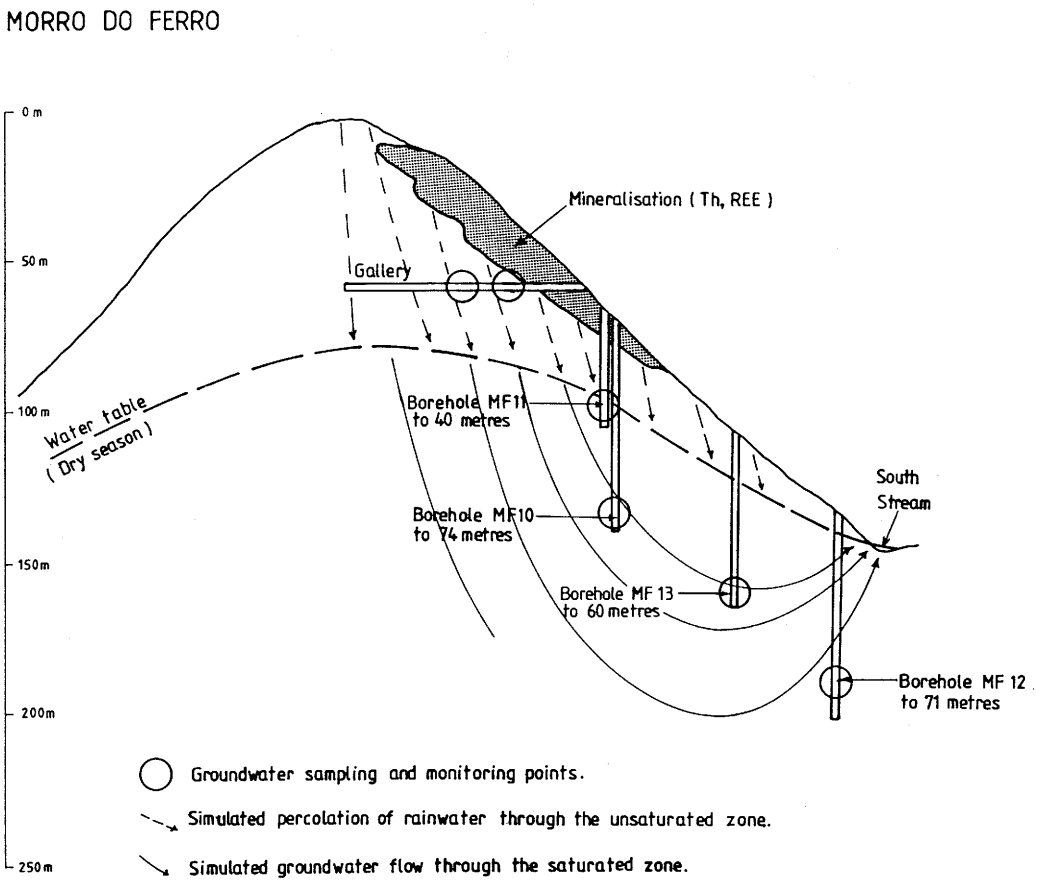

Figure 4. Cross-section of Morro do Ferro showing the borehole locations in relation to the mineralisation and the groundwater flow gradients.

2) Seasonal sampling four times a year (wet and dry seasons and transitional periods) for complete major and trace element and isotopic analyses. Additional samples for colloid and microbiological studies were taken in parallel.

A number of precautions were taken to minimise groundwater contamination during drilling, for example using water for drill-flushing of similar composition and redox character to the groundwaters expected to be intercepted at depth. In addition, borehole completion was carried out as soon as possible after drilling, to prevent any serious open-hole cross-circuiting groundwater flow effects.

Water samples were pumped from boreholes, or were collected by artesian flow when conditions permitted, through nylon sampling tubes from single packer systems at specified depths. After pumping for approximately 2 hours to ensure a representative groundwater composition, samples were filtered through 0.45 micrometre membranes in a plexiglass unit for laboratory analyses. Cation analyses were made on samples acidified with concentrated HCl (to a sample concentration of 1%). Measurements of pH, temperature, Eh and conductivity were made on-site by pumping the water through a flow-cell arrangement closed to the atmosphere.

Analyses of the groundwaters were carried out on-site for the twice-weekly routine sampling, and at a series of Brazilian and international laboratories for the major seasonal hydrochemical programme. Using these analyses, a rigorous quality evaluation was carried out, eventually resulting in the identification of a selected set of representative analyses for groundwater characterisation and modelling purposes.

4. Computational strategy and methods

The chemical model computations in this report were performed using the strategy developed and described by Plummer *et al.* (1983). These concepts have been further elaborated on by Plummer (1984) as the inverse and forward methods of chemical modelling of natural waters. The strategy can be simply described as follows. For a groundwater system, sampling points along a flow path will show progressive changes in chemical and isotopic properties. These changes reflect geochemical processes such as mineral dissolution and precipitation, ion exchange, gas exchange and oxidation-reduction reactions. The first obvious constraint on these processes is the chemical and isotopic data-set itself. The next constraint is the tendency of the groundwater to dissolve or precipitate minerals as reflected by the saturation indices that are obtained from

speciation calculations based on the water analyses. Speciation calculations require the use of an aqueous chemical model that must be known to be reliable for the specific conditions of application. The next step, and perhaps the most critical one in the strategy, is the determination of one or more "non-thermodynamic" reaction models that can account for the changes in water chemistry between any two points along a flow path by mass balance calculations similar to those first described by Garrels (1967) and Garrels and MacKenzie (1967). The mass balance calculation is done by simultaneously solving a set of equations that relates the change in elemental composition to several possible reactions according to their assumed stoichiometry. In a sense, it is a matrix transformation from compositional changes in aqueous constituents to mass transfer changes in minerals, gases and redox conditions using the stochiometry of the phases to make the transformation. Plummer (1984) describes this step as the inverse method because one is working backwards from the water composition to the assumed processes responsible for that water composition. Finally, when one has arrived at a most probable model or set of models within the constraints of the saturation indices and available chemical and isotopic data, a check on the thermodynamic feasibility of any model can be carried out by the forward method. This method can assume the saturation and mass balance constraints obtained in the inverse method so that the results are more likely to be successful. The forward method then provides the complete thermodynamic description of the system and can better describe where equilibrium is not reached and kinetic information is needed.

Speciation calculations were made to determine saturation indices and to make redox potential calculations. The saturation index of a particular mineral, 'i', is defined by

$$SIi = \log \frac{IAPi(T)}{Kspi(T)}$$

where IAPi(T) is the ion activity product of 'i' as a function of temperature and Kspi(T) is the solubility product constant of 'i' as a function of temperature. Saturation indices describe the thermodynamic tendency of a water to dissolve or precipitate various minerals. They are based on the water composition, the equilibrium constants for aqueous complexing reactions and activity coefficients for correcting to a common reference state. More details are found in Drever (1988) and in Nordstrom and Munoz (1986).

The full water analyses for major and trace elements and a summary of the chemical characteristics of the groundwater are found in Nordstrom *et al.* (this report series;

Rep. 6). Fe (II/III) analyses were used to speciate ferrous and ferric iron and to calculate an Eh based on the Nernst equation.

Three computer programs were utilised to carry out the inverse and forward methods of geochemical modelling. Speciation calculations were performed with the WATEQ4F program (Ball *et al.*, 1987, 1990) using the revised database of Nordstrom *et al.* (1990). Mass balance models of rock/water interactions were calculated with an interactive version (BALINPT) of the BALANCE program (Parkhurst *et al.*, 1982). Thermodynamic mass transfer calculations were performed with the PHREEQE program (Parkhurst *et al.*, 1980), using the same revised database as in the WATEQ4F program.

5. Investigation of CO_2 degassing and iron oxidation

There are several discrepancies between laboratory and field pH values (see Table I). Chemical equilibrium calculations with the PHREEQE and WATEQ4F programs show that field pH measurements in combination with water analyses give calculated equilibrium partial pressures of $CO_2(g)$ that are higher than the average atmospheric value. Degassing of the groundwaters can therefore take place after sampling. This process will increase the pH values measured in the laboratory (Pearson *et al.*, 1978) due to the reaction:

$$HCO_3^- \rightarrow CO_2(g) + OH^-$$

The effect of CO_2 degassing on the laboratory pH measurement was simulated with a series of calculations in which the groundwater samples were equilibrated with atmospheric CO_2. The results are presented in Table II and show that CO_2 degassing may result in a pH increase of up to 1.7 pH-units. This confirmed the samples to be supersaturated with respect to atmospheric CO_2.

In addition to the effects of CO_2 degassing discussed above, Fe(II) in groundwater samples will be oxidised with atmospheric oxygen, as indicated by the reaction:

$$2.5\ H_2O + Fe^{2+} + 0.25\ O_2(g) \rightarrow Fe(OH)_3(s) + 2\ H^+$$

TABLE I

Representative groundwater analyses.

(concentrations in mg/L)

	F1	F2	F4	MF12
Code	[Select]	PC-GW-78	PC-GW-80	PC-GW-50
Date	870707	890320	890413	880614
T °C	22	21	24	21
pH(field/lab)	4.87/4.06	5.90/6.42	5.83/6.38	5.99/6.19
Eh	338	191	462	212
Alkalinity	2.0	10	23.5	22
Ca	0.47	2.65	7.88	8.48
Mg	0.07	0.07	0.46	0.70
Sr	0.043	0.009	0.20	0.346
Ba	0.125	0.13	0.12	<0.001
Na	0.20	0.2	0.63	0.84
K	12.7	13.5	11.8	11.2
Fe(II)	1.30	1.67	6.13	0.74
Fe(III)	1.33	1.70	6.27	0.79
Al	<0.05	0.319	0.183	0.21
Mn	0.19	0.318	0.13	1.68
Zn	0.083	0.211	2.17	0.27
SO_4	16	14	28	9.5
F	0.41	2.57	6.0	5.3
Cl	3.0	<2	<2	<0.1
Br	0.04	<0.05	<0.05	<0.05
SiO_2	35	29	34	33.4

TABLE II

Results of PHREEQE calculations simulating CO_2(g) degassing of selected samples.

		initial values			Calc.	Meas.
		pH	Alk.	log P_{CO_2}	final-pH	lab-pH
Sample	date	(field)	mg/L	atm		
Morro do Ferro:						
MF12						
PC-GW-50	880614	5.99	30.0	–1.698	7.94	6.55
		5.99	25	–1.777	7.86	6.55
		5.99	22	–1.633	7.80	6.55
Osamu Utsumi uranium mine:						
F1						
PC-GW-42	880601	5.25	3	–1.751	6.93	5.51
F1						
PC-GW-42	880601	5.25	4.3	–1.595	7.11	5.51
F2						
PC-GW-43	880602	5.72	6	–1.921	7.13	6.08
F3						
PC-GW-95	880606	5.21	3	–1.764	6.40	6.06

This reaction will both acidify the samples and increase the degassing process, giving the overall reaction:

$$0.5\ H_2O + Fe^{2+} + 0.25\ O_2(g) + 2\ HCO_3^- \rightarrow Fe(OH)_3(s) + 2\ CO_2(g)$$

Experiments were performed in order to quantify the relative influence of these reactions on samples from Poços de Caldas. Groundwaters were sampled from boreholes F1 and F3 (mine reference 9-1WC11 and 9-1NH47 respectively) from the Osamu Utsumi uranium mine. Field values of pH and Eh were measured and the waters were filtered through a 0.45 μm membrane filter before transportation to the laboratory, where Fe(II) and total iron were determined.

Air was then bubbled continuously for about 500 hours through the groundwater samples which were contained in plastic bottles. To avoid contamination of the samples with suspended particles in the gas, the air was forced through a wash-bottle containing distilled water before it was introduced into the groundwaters. Samples were taken at time intervals for pH, Eh and $Fe(II)/Fe_{tot}$ determination (after filtration through 2 μm filters). Some of the results are shown in Figures 5 and 6, which show pH and total iron concentrations as a function of time for the groundwaters F1 and F3.

Chemical equilibrium calculations were made with the PHREEQE program to see whether the observed data correspond to the expected processes of CO_2 degassing and Fe(II) oxidation. Experimental alkalinity and field pH were used to calculate the initial chemical state of the "undisturbed" groundwater. This calculation gives values for total inorganic carbon, equilibrium partial pressure of $CO_2(g)$, etc. The groundwater was then allowed to equilibrate with atmospheric $CO_2(g)$ by entering a partial pressure of $3.16 \cdot 10^{-4}$ atm and calculating the resulting pH and chemical composition. This result was used for the subsequent calculations simulating Fe(II) oxidation. Judging from the experimental data collected, the CO_2 degassing process was relatively fast in the experiments (maximum pH change is achieved in about 24 hours). The diffusive transfer of oxygen from air to the groundwater probably takes place within the same time period. This implies that, after about 24 hours, the groundwater samples were saturated with atmospheric oxygen ($2.6 \cdot 10^{-4}$ mol/L).

Iron(II) oxidation by the dissolved oxygen was clearly a slower process. Half-times reported in the literature for natural waters are in the range 3 minutes to 23 hours (Sung and Morgan 1980; Millero *et al.*, 1987). In the two cases studied here, the half-life of Fe(II) is in the order of a hundred hours (see Figs. 5 and 6). This might be due to a lower pH, or to the presence of some organic complexing agent (Theis and Singer, 1974).

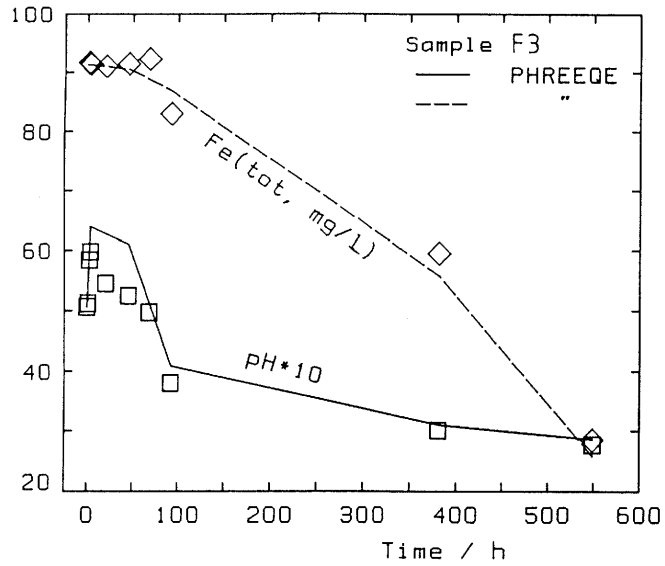

Figure 5. Changes in pH and dissolved iron concentrations during degassing and oxidation of a sample from F3 as measured (open symbols) and calculated from the PHREEQE program (pH = solid line, iron = dashed line).

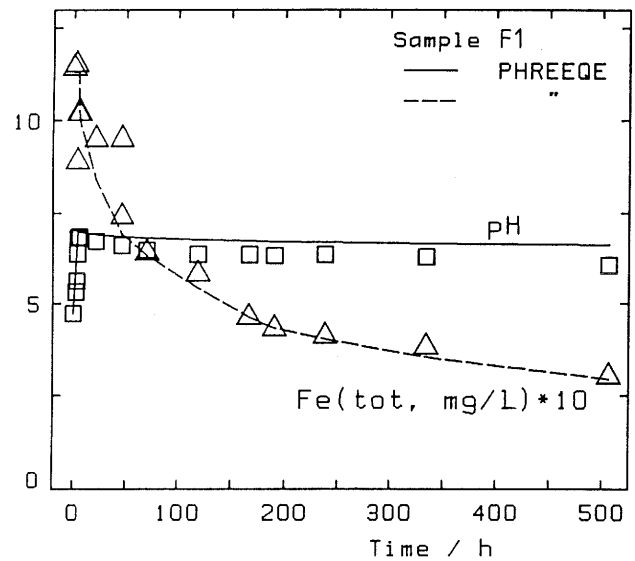

Figure 6. Changes in pH and dissolved iron concentrations during degassing and oxidation of a sample from F1 as measured (open symbols) and calculated from the PHREEQE program (pH = solid line, iron = dashed line).

The oxidation simulation of Fe(II) by dissolved oxygen through a series of chemical equilibrium calculations performed with the PHREEQE program has been carried out as follows. For each value of Fe(II) (measured as a function of time), the equivalent quantity of oxygen was added to the aqueous solution previously saved from the CO_2 degassing calculations. The PHREEQE program assumes redox equilibrium and it was specified that the solutions should be equilibrated with ferrihydrite and that the pH should be calculated as function of reaction progress.

The results are shown in Figures 5 and 6. They show that CO_2 degassing may result in a pH increase of up to 2 pH-units for dilute, unbuffered groundwaters (i.e. F1). For waters more concentrated in dissolved components, the pH increase due to degassing is more limited and the effect of Fe(II) oxidation is larger for the most concentrated solutions, as they contain more reduced iron, giving rise to a net decrease in pH as is the case for F3.

6. Results and discussion

The chemical composition of the waters at Poços de Caldas is influenced by processes including CO_2 exchange, secondary mineral formation and redox reactions. Weathering of rock minerals will consume incoming acidity (CO_2 introduced in the recharge area), release alkaline and alkaline earth cations and induce the precipitation of secondary minerals (kaolinite, montmorillonite, silica, etc).

Although the driving force is made up of differences in thermodynamic potentials, the chemical composition of natural waters is often regulated kinetically, so that chemical equilibrium between groundwaters and rock minerals is not always reached. Therefore, hydrological parameters that influence the residence time of groundwaters in the bedrock are also reflected in the chemical composition of the waters.

Geochemical mass balance calculations may be used to make quantitative analyses of major element transfer between groundwaters and minerals. Together with hydrological parameters, this allows estimations of reaction rates in a given aquifer system (Plummer and Back, 1980; Plummer *et al.*, 1983).

In this study, the BALANCE program has been used to characterise the reactions influencing the chemical composition of the waters in the Poços de Caldas region. This program creates input-output budgets which consist of total amounts of minerals dissolved and/or precipitated along a reaction path. However, these models might not be reasonable when equilibrium constants and aqueous concentrations are considered,

i.e. the dissolution or precipitation reactions might be thermodynamically impossible. Therefore, the PHREEQE program has been used to check the thermodynamic feasibility of the budget models obtained with BALANCE.

The geochemical evolution of groundwaters at Morro do Ferro and at the Osamu Utsumi mine can be interpreted by examining ion plots, saturation indices and mass balance calculations. Ion plots provide a convenient method of organising the water chemistry data and, when combined with plots of saturation indices, they indicate which water/mineral reactions may dominate. The initial model of geochemical processes is formulated with the interpretation of these plots. Modification and expansion of the model follows from mass balance calculations and final confirmation of the model is achieved by thermodynamic mass transfer calculations.

6.1. Processes deduced from ion plots and mineral saturation indices

In the following diagrams all the water analyses with charge imbalances less than 30% were used for plotting purposes. The distribution of charge imbalance as shown in Figure 7 indicates a high degree of reliability for most analyses.

Some mineral/water reactions demonstrate a very clear equilibrium solubility control. One of the best examples is barite solubility as shown in Figures 8 and 9; a classic example of the common-ion effect on solubility is shown in Figure 8. Up to about 10 mg SO_4/L, barite is undersaturated. Above this sulphate concentration, the Ba concentrations increase by more than two orders of magnitude. Continuing to higher SO_4 concentrations, the Ba concentrations decrease regularly in a pattern parallel to the common-ion effect on barite solubility, seen when SO_4 is added (shown by the dashed line representing experimental measurements of barite solubility in Na_2SO_4 solutions). The field data show supersaturation compared to the experimental data. The amount of supersaturation is also seen clearly in Figure 9 where the saturation index (SI) of barite is plotted against the SO_4 concentrations. This amount of supersaturation, up to a half order of magnitude, cannot be explained by analytical errors or errors in the thermodynamic data (Nordstrom and Ball, 1990). Two possible reasons are:

1) The effect of degree of crystallinity on solubility where high surface areas and/or surface defects enhance the solubility.

2) Enhancement due to solid solution solubility behaviour or contaminant substitution effects.

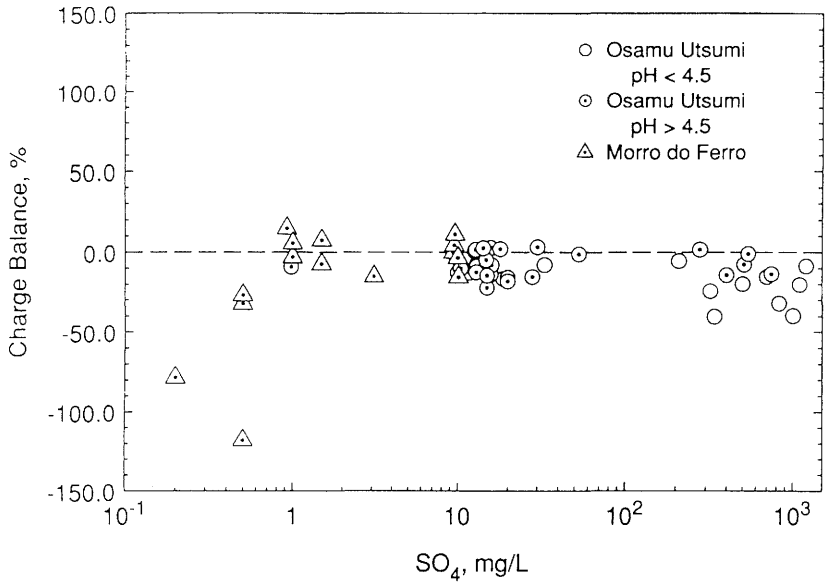

Figure 7. Charge balance distribution as a function of sulphate concentrations.

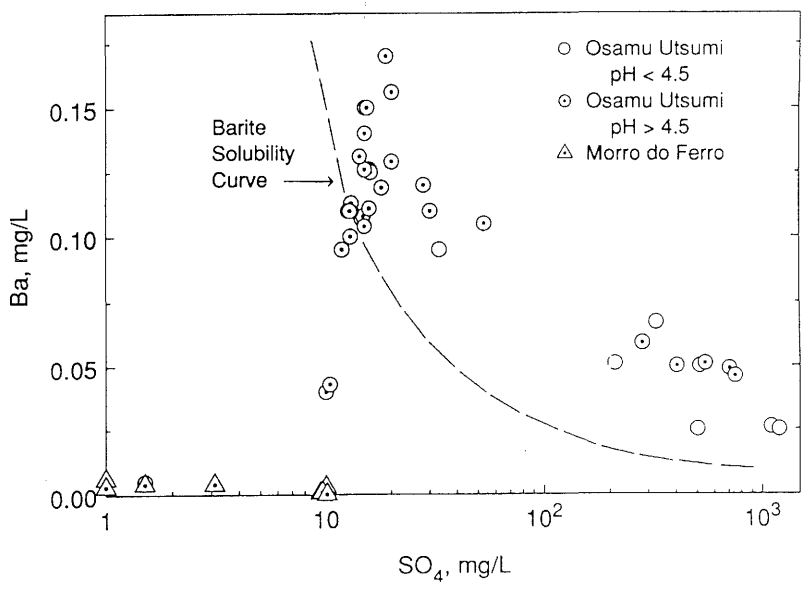

Figure 8. Common-ion effect of increased sulphate concentrations from pyrite oxidation on the solubility of barite. Symbols represent field data and dashed line shows experimental measurements of barite solubility in the presence of sodium sulphate solutions.

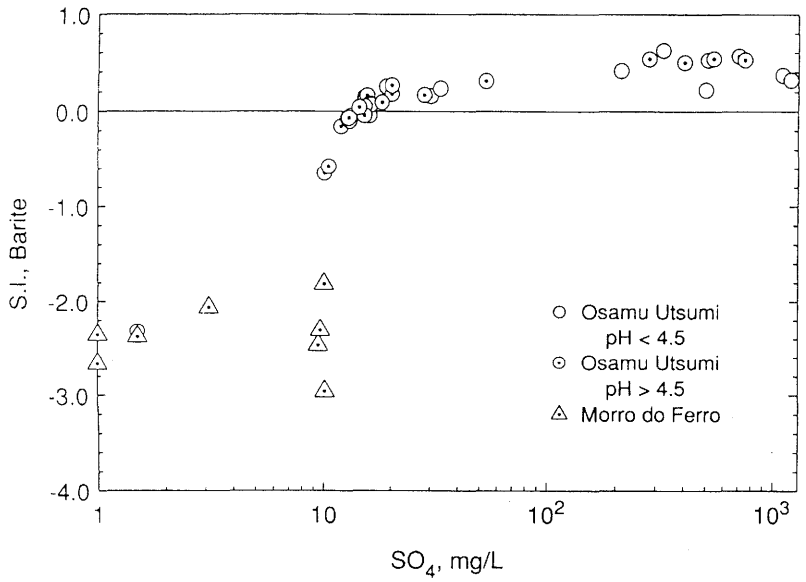

Figure 9. Barite saturation indices plotted against sulphate concentrations demonstrating stoichiometric solubility control but at a consistent level of supersaturation.

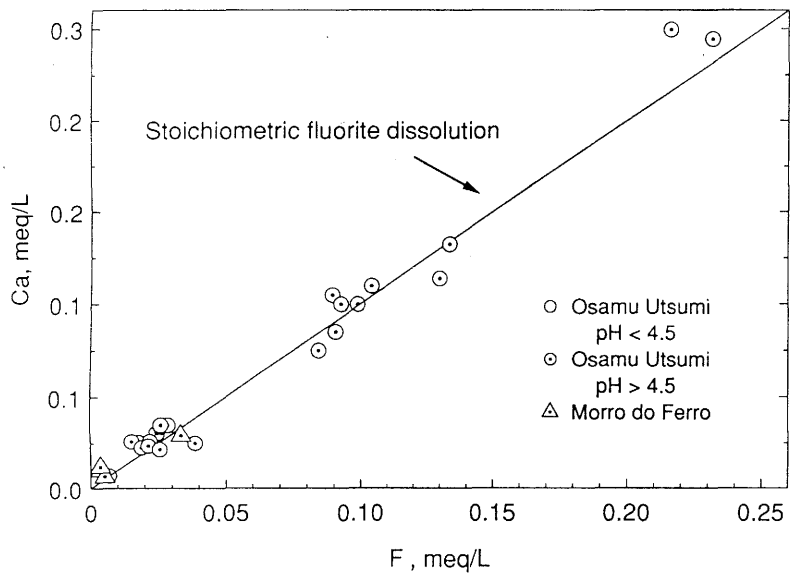

Figure 10. Calcium concentrations plotted against fluoride concentrations for the more dilute waters showing the quantitative agreement with fluorite dissolution as the dominant source of these ions.

If colloidal barite were the cause of an apparent supersaturation, then at least some of the values should show equilibrium saturation because it seems likely that at least a few water samples would not have carried significant quantities of colloidal barite (as can be seen in the case of ferrihydrite). Furthermore, SEM pictures of secondary barite along weathered fracture surfaces clearly show well-crystallised blades greater than 1 micrometre in diameter. Solid solution solubility could be a possibility, but barite is usually a fairly clean mineral with limited solid substitution. Strontium and radium are the most likely candidates that must be further examined. Hence, it appears that the supersaturation may be real and implies a faster rate of Ba or SO_4 input to the water than can be removed by precipitation of barite near equilibrium. It is quite possible that the rate of sulphate supply by pyrite oxidation is faster than barite precipitation near equilibrium.

Calcium and fluoride concentrations are often present in amounts identical to the stoichiometric ratio for fluorite, as seen in Figure 10. The very close approach of the data points to the line representing fluorite dissolution demonstrates that all of the calcium and fluoride concentrations can be accounted for by the dissolution of fluorite for the more dilute waters. Figure 11 displays the higher concentration waters and shows significant deviation from fluorite stoichiometry due to Ca enhancement, primarily in the F3 borehole waters. This enhancement might be due to calcite dissolution or mixing with acid mine waters or both. Some of the acid mine waters also show enhanced Ca/F ratios. These acid waters would leach Ca more readily from residual clay minerals and from relatively insoluble accessory minerals than would neutral pH waters.

Saturation indices for fluorite are plotted in Figure 12, demonstrating that several water samples reach saturation equilibrium, but most are undersaturated and indicate a tendency to dissolve fluorite.

Strontium is usually derived from the same source as calcium and, consequently, concentrations were expected to correlate with Ca concentrations. The plots of Sr concentrations against Ca concentrations in Figure 13 for the low concentration waters and Figure 14 for the high concentration waters show a greater proportion of Sr relative to Ca (1–10%). Fluorites rarely ever contain more than 0.5% Sr (Steyn, 1954). Calcites may contain up to 10% Sr, but calcite is not such a major contributor to the Ca content of the water as discussed above. Since the primary rock is rather high in Sr, and secondary Sr minerals such as goyazite ($SrAl_3(PO_4)_2(OH)_5H_2O$) are known to occur, it seems likely that the source of strontium may be dominated by minerals other than fluorite and calcite.

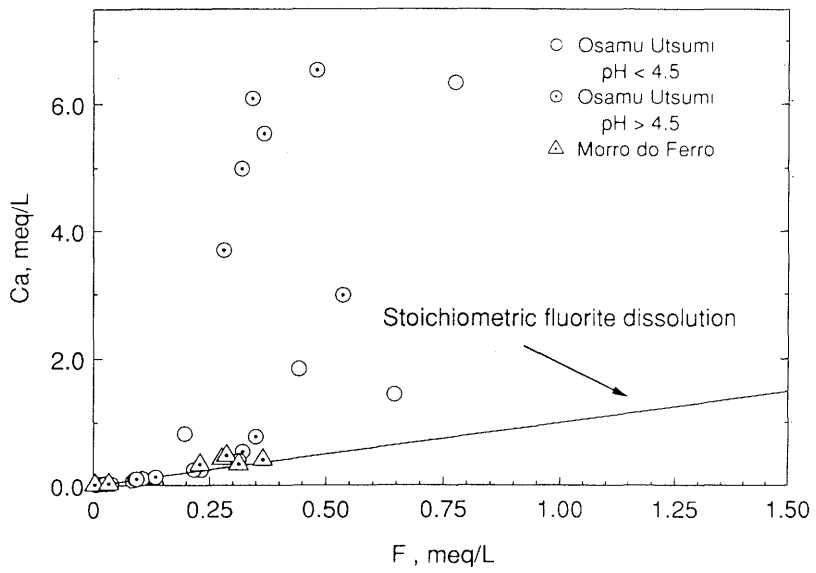

Figure 11. Calcium concentrations plotted against fluoride concentrations for all water samples showing calcium enhancement above fluorite dissolution for the higher concentration samples.

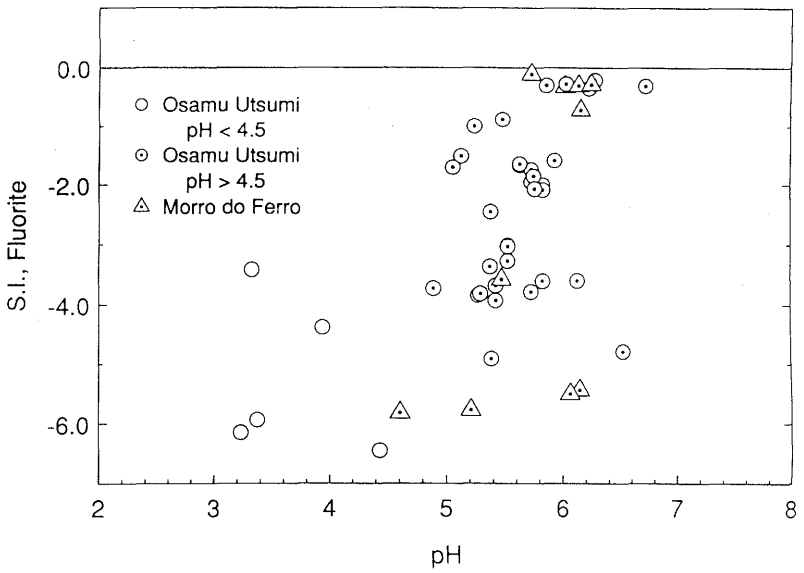

Figure 12. Fluorite saturation indices plotted against pH.

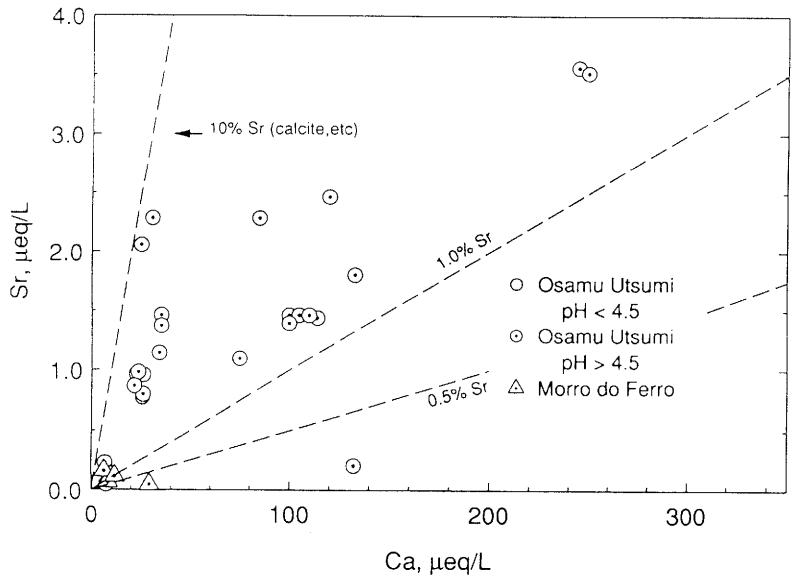

Figure 13. Strontium concentrations plotted against calcium concentrations for the dilute waters.

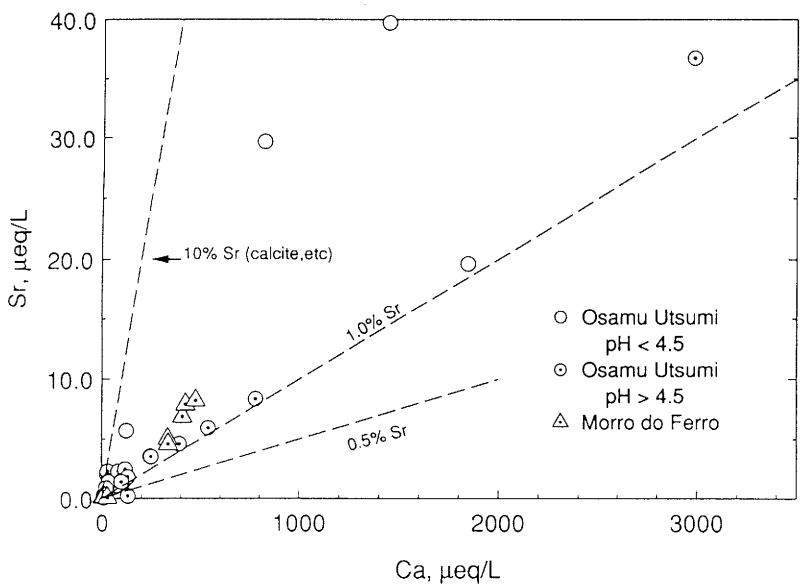

Figure 14. Strontium concentrations plotted against calcium concentrations for all waters.

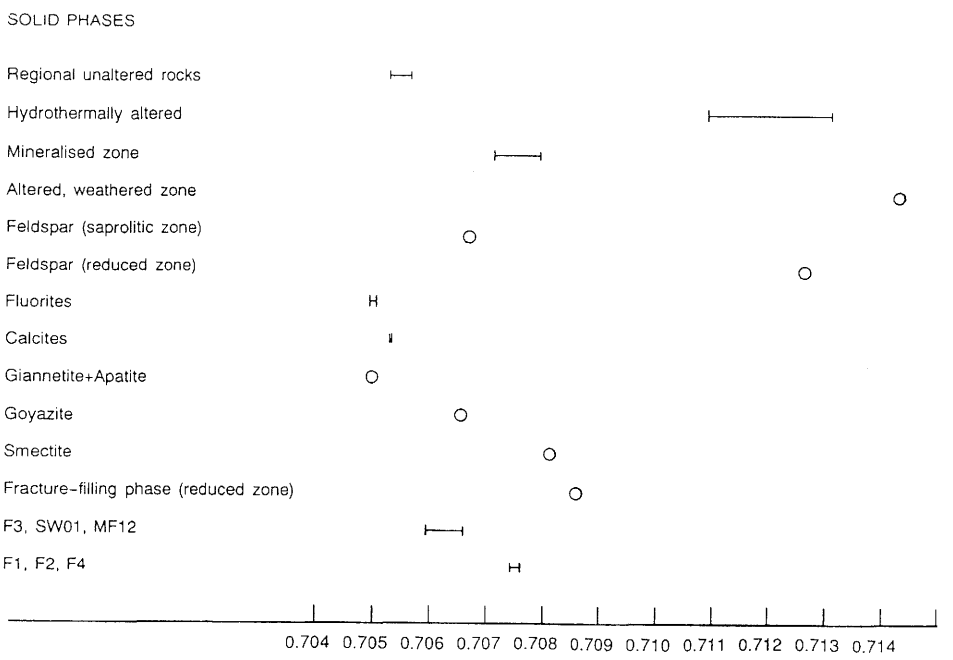

Figure 15. Strontium isotope data. Values along the bottom are $^{87}Sr/^{86}Sr$ isotope ratios.

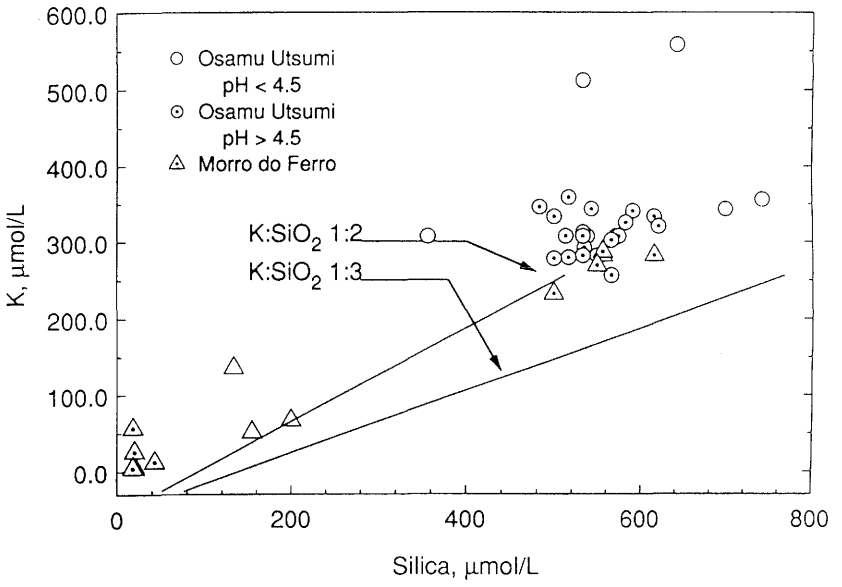

Figure 16. Concentrations of potassium plotted against silica.

The strontium isotope data summarised in Figure 15 support and expand the hypothesis developed above. The Sr-87/86 ratios of the groundwaters fall into two groups with the deeper or more strongly leaching waters (acid mine waters) averaging about 0.7060 and the younger, more dilute waters averaging about 0.7075. The regional primary rocks, mostly nepheline syenites, have mantle-influenced signatures of about 0.7052 with a shift to heavier values of 0.7125 upon hydrothermal alteration (Shea, this report series; Rep. 4). These extremes in Sr-87/86 bracket the ratios for the groundwaters as well as the ratios for K-feldspar and a few secondary minerals (goyazite, giannetite, smectite). However, of the analysed crystal phases, only the K-feldspar (weathered saprolitic zone), goyazite, and, marginally, smectite and a fracture-filling mineral phase, match the groundwater isotope ratios. This supports the hypothesis that calcites and fluorites are not major sources of strontium, whilst K-feldspar, not unexpectedly, is a major supplier. It is still not clear whether the "fresh" K-feldspar (reduced zone) or the K-feldspar alteration products (i.e. clays, smectites) are the direct supply of strontium to the groundwater. The "fresh" K-feldspar cannot be the only source ($^{87}Sr/^{86}Sr$ value is too high) and, if the alteration products are considered, then most of the Rb and radiogenic ^{87}Sr (formed on the Rb site in the crystal lattice) must have been removed at the time of feldspar alteration. If subsequent equilibration occurred between the water and the altered K-feldspar products, the water would now have a more "common" Sr signature, similar to that of the "fresh" feldspar. That it does not, shows that K-feldspar is not the only source for the strontium. Therefore, the sources are a mixture of several phases rich in strontium including, in addition to K-feldspar, goyazite, smectite, nepheline and some calcite and fluorite.

The groundwaters are characteristically high in K and SiO_2, reflecting the strong potassic alterations, the highly weathered nature of the rock and the mildly to strongly acidic solutions developed at the field sites. The main source of potassium and silica for these groundwaters is K-feldspar, illite/sericite and possibly felspathoids typical of nepheline syenites. If K and SiO_2 are simply leached out of these minerals congruently, then the K/SiO_2 ratio should reflect the source-mineral stoichiometry.

The K and SiO_2 concentrations plotted in Figure 16 suggest that minerals more potassic-rich than feldspar are responsible for these constituents. The difficulty with such an interpretation is that the high and consistent silica concentrations (Fig. 17) may indicate a solubility control. Solubility control by a phase approximating alpha-cristobalite is suggested by the data in Figure 17. Alternatively, the constant silica concentrations (for all but recharge waters) may reflect a steady-state balance between

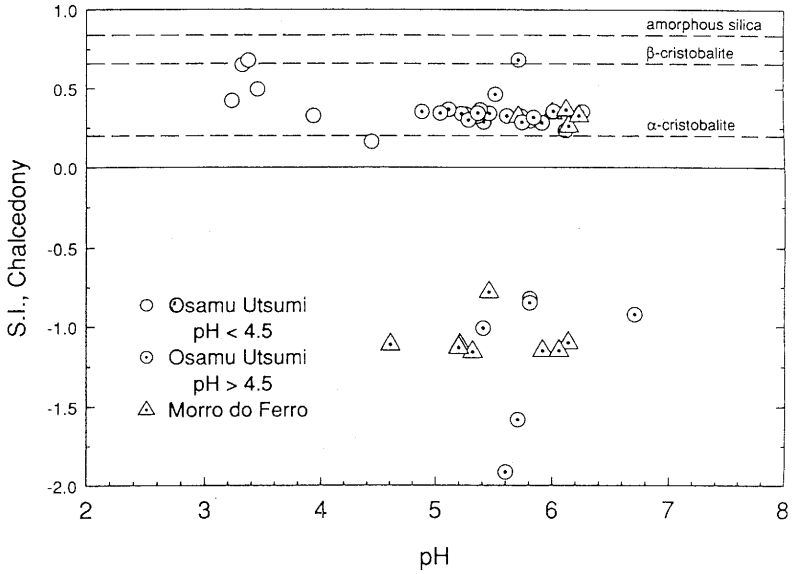

Figure 17. Silica saturation indices (as S.I., chalcedony) plotted against pH concentrations.

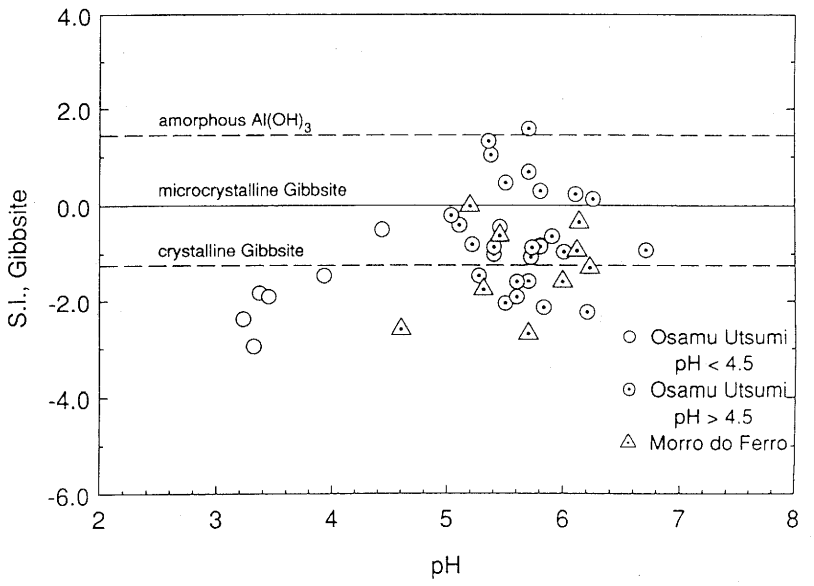

Figure 18. Gibbsite saturation indices plotted against pH.

the rates of K-feldspar dissolution and kaolinite precipitation. This question will be explored further in the mass balance discussion.

In a highly-weathered, aluminium-rich environment such as that in the weathered zones at Poços de Caldas, solubility equilibrium would be anticipated for gibbsite and kaolinite. The saturation indices for gibbsite and kaolinite plotted in Figures 18 and 19 show that many of the waters have reached saturation equilibrium within the range expected for poorly-crystallised varieties of these minerals. There is not, however, the clear pattern of stoichiometric organisation of the data points as seen for barite and silica. This result could reflect the difficulty in analysing for truly dissolved aluminium. Colloidal particles containing aluminium probably pass through the 0.45 micrometre filter membranes. In addition, if Ostwald ripening of clay particles is taking place, there should be a spread of saturation indices over the range of grain sizes known to occur.

A noteworthy feature in Figures 18 and 19 are the undersaturation effects for pH<4.5. A more likely stable mineral solubility under these conditions is alunite. The saturation indices for alunite as a function of SO_4 concentrations in Figure 20 and pH in Figure 21 suggest saturation is reached for alunite in the more acid higher-sulphate waters.

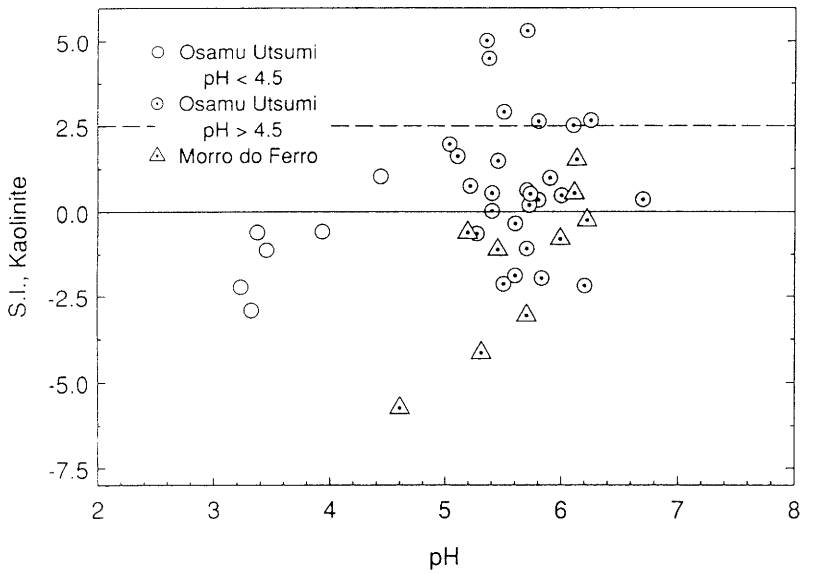

Figure 19. Kaolinite saturation indices plotted against pH.

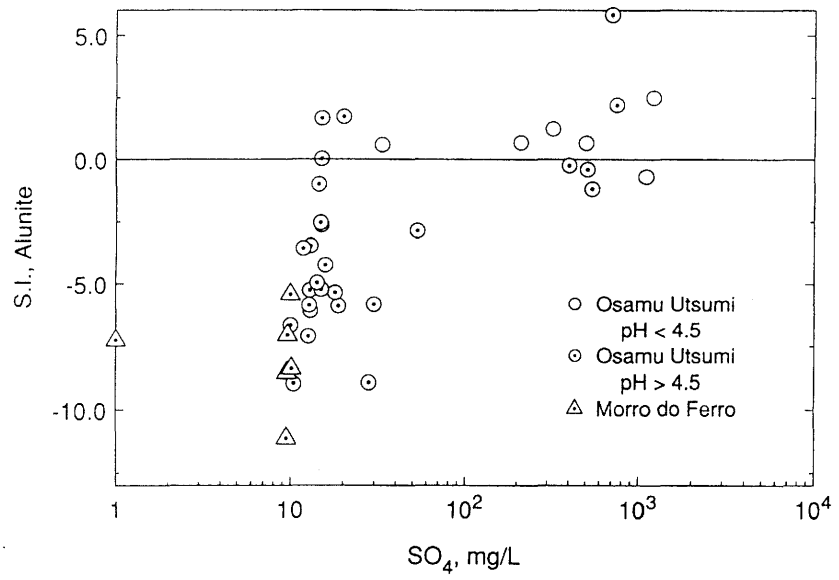

Figure 20. Alunite saturation indices plotted against sulphate concentrations.

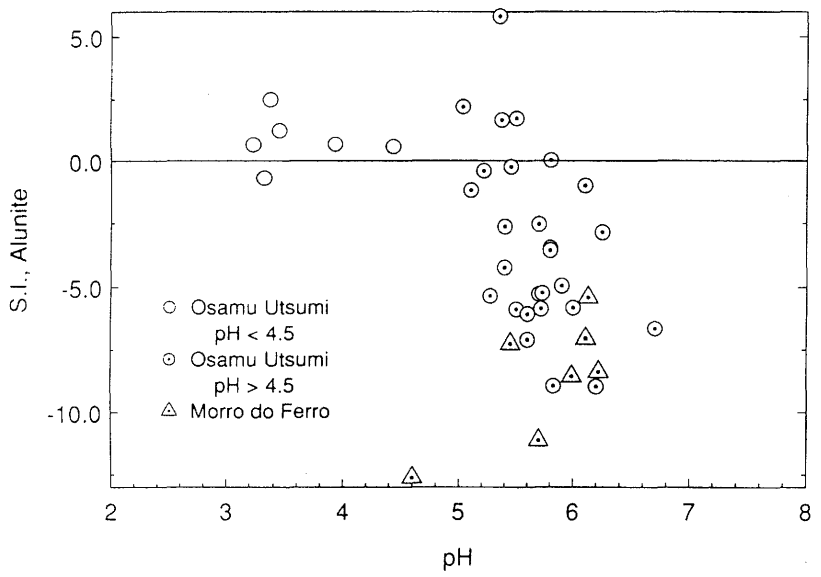

Figure 21. Alunite saturation indices plotted against pH.

6.2. Redox potential measurements and Fe and Mn chemistry

A comparison of the redox potential measured by the platinum electrode with that calculated from the Fe(II/III) determinations is shown in Figure 22. About a dozen data points are in excellent agreement, indicating the reversible response of the platinum electrode to the iron redox couple. Since the iron concentrations are reasonably high in most of these waters, however, better agreement for more of the data was anticipated. A strong bias towards higher Fe(III) concentrations than needed for a reversible potential is indicated by the data. This bias might occur if colloidal ferric oxyhydroxides (ferrihydrite) were passing through the filtration device. Demonstration of ferrihydrite colloids in the 20–100 nm range has been documented by B. Kimball (pers. comm.) for acid mine waters. This possibility finds considerable support in Figure 23 where the ferrihydrite saturation indices are plotted. Supersaturation of 1–2 orders of magnitude is not reasonable from the experimental behaviour of freshly precipitating ferrihydrite. The best current explanation for this apparent supersaturation is the inclusion of ferrihydrite particles in the Fe(III) determinations.

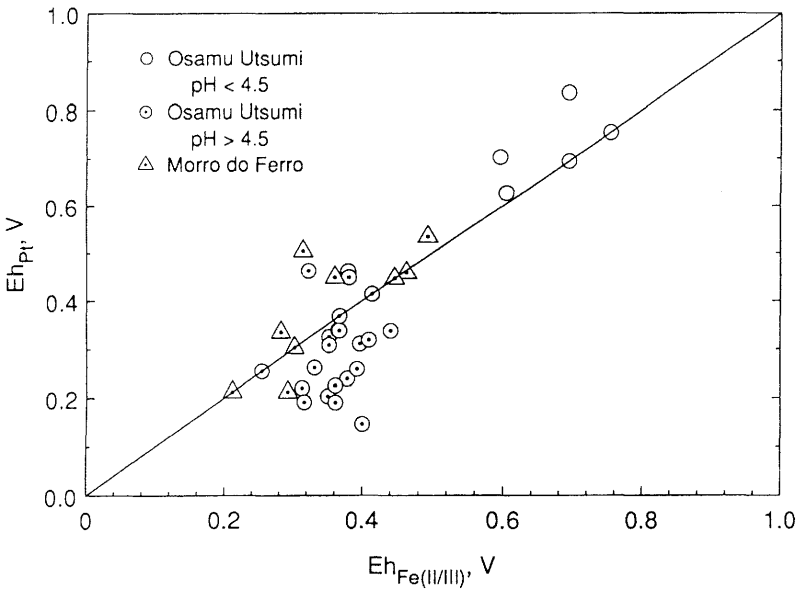

Figure 22. Comparison of measured Eh from platinum electrode EMF measurements with Eh calculated from Fe (II/III) determinations.

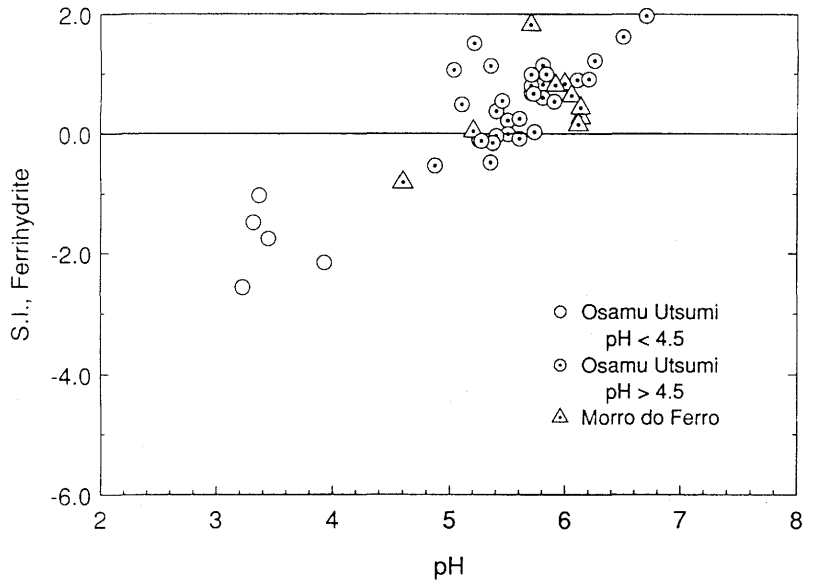

Figure 23. Ferrihydrite saturation indices as a function of pH.

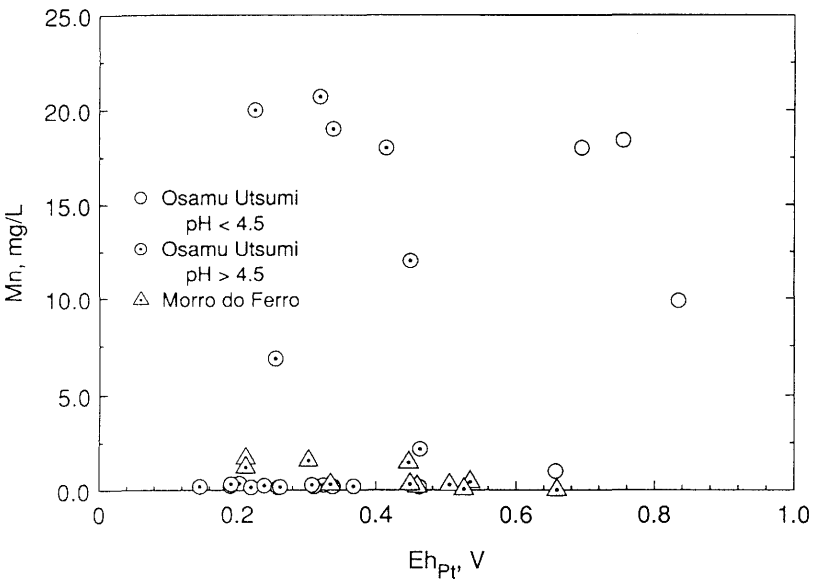

Figure 24. Manganese concentrations plotted against Eh.

Manganese concentrations in groundwaters are sensitive to changes in redox chemistry, being very insoluble under oxidising conditions and much more soluble under mildly reducing conditions. Consequently, manganese concentrations should show increases with decreasing redox potential. The data plotted in Figure 24 do not show a clear trend as expected. The highest concentrations are either F3 values or acid mine waters. If the Osamu Utsumi mine site values are excluded and just the Morro do Ferro values considered, the expected trend is more apparent, with manganese concentrations increasing when redox potentials decrease below about 450 mV.

6.3. Geochemical evolution of groundwater at Morro do Ferro

At this site the groundwater is much less perturbed compared to the Osamu Utsumi mine. Iron and fluoride concentrations at about 70 m depth are very comparable to those in the deep groundwaters at the mine, whereas uranium, bicarbonate and sulphate concentrations appear to be slightly lower and the pH slightly higher. These differences in water chemistry may reflect a less perturbed groundwater flow system, a lower abundance of oxidisable pyrite and/or stronger reducing conditions.

The MF12 sample has been selected for this area as a representative water with a high residence time underground (i.e. with a chemical composition representative of a high degree of bedrock weathering and probably in equilibrium with secondary minerals). The recharge waters are, in general, so dilute that pure water was used as an initial aqueous phase for the mass balance calculations.

The result from the BALANCE program is shown in Table III. For the reaction path simulation with the PHREEQE program (reported in the same Table), a constant and relatively high redox potential (Eh$\approx$+230 mV) was used throughout the simulation. This is necessary in order to achieve pyrite dissolution and goethite precipitation and it is consistent with the general range of platinum electrode measurements at this site. Furthermore, as the PHREEQE database used includes carbonate as a redox active species, the calculated redox potentials would be affected by calcite precipitation if the Eh was not kept constant. Some CO_2(g) was added to simulate the high partial pressures of CO_2 usually encountered in root-soil waters of recharge areas. This was necessary to achieve a reasonable final pH in the PHREEQE calculation and is not in contradiction with the BALANCE model as it does not take pH differences into consideration.

TABLE III

Mass balance and mass transfer results for the MF12 borehole (Morro do Ferro, selected reference water sample) using the programs BALANCE and PHREEQE. Results in mmol/kg of substance dissolved (positive) or precipitated (negative values).

Substance computed	BALANCE	PHREEQE
Fluorite	0.140	0.140*
Calcite	0.072	0.072*
K-spar	0.2865	0.2865*
Albite	0.0365	0.0365*
Kaolinite	–0.1576	–0.377
Chalcedony	–0.0978	–0.156
Pyrite	0.056	0.056*
Sphalerite	0.004	0.004*
Ferrihydrite	–0.0428	–0.043
MnOOH	0.0306	0.0306*
$CO_2(g)$	–	1.00
pH	5.99[1]	6.05
log P_{CO_2}	–1.66[2]	–1.68
Eh	3.63[1]	–3.94

*These values were taken directly from the BALANCE model.

[1]Field measurements.

[2]Computed from pH and alkalinity with WATEQ4F.

A note of caution is needed when referring to Table III. The calculated amount shown for Fe(III) hydroxide precipitating depends both on the redox potential and on the logarithm for the solubility product constant for ferrihydrite.

$$Fe(OH)_3(s) + 3\,H^+ \rightleftarrows Fe^{3+} + 3\,H_2O$$

which has values in the range 3 to 5 depending on the degree of crystallinity (Nordstrom *et al.*, 1990). For any given redox potential in the range +170 to +285 mV, an equilibrium constant can be selected that gives the desired amount of solid precipitated in the PHREEQE calculation.

The results in Table III show that, assuming the mass balance model as given, the results are thermodynamically permissible. This is further demonstrated by the excellent agreement of the calculated values for pH, log P_{CO_2}, pe and mass of minerals precipitated. These values were not set by the BALANCE results but were an outcome of the mass transfer calculations, assuming only that equilibrium is reached with those minerals listed that reach saturation.

6.4. Geochemical evolution of groundwater at the Osamu Utsumi mine

The analytical results from the Osamu Utsumi mine boreholes reflect an unusual groundwater chemistry that suggests intense weathering from actively circulating fresh groundwaters in contact with a highly-leached potassic-rich rock mass. The major cation is potassium, which is present at an order-of-magnitude greater concentration than any other cation. Rarely does any other cation achieve a concentration greater than 1 mg/L, whereas potassium is consistently about 10 mg/L. Another unusual feature is the frequent occurrence of barium concentrations greater than those of strontium and sometimes as high as the calcium concentrations. Iron concentrations are also quite high, up to 2 mg/L, and mostly as Fe(II). Aluminium concentrations are elevated because of the moderate acidity reflected by the pH values. Zinc concentrations also tend to be elevated, probably reflecting the oxidation of sphalerite which sometimes occurs in mineralised zones, along with pyrite.

The highest concentrations of iron, uranium, fluoride and sulphate are found at the surface and in the shallow auxiliary boreholes (10 m depth). These waters also exhibit the lowest pH and low alkalinity. Pyrite is dispersed throughout the hydrothermally altered rock, and oxidation of the pyrite has produced acid mine water at and near the surface. Fluorite is a common fracture mineral at the mine and acid leaching has caused an increase in fluoride concentration in surface and near-surface waters. With depth, the concentrations of iron, uranium, fluoride and sulphate all decrease and the pH and alkalinity increase. Typical groundwaters below 20 m range in pH from 5–6 and contain 10–30 mg HCO_3/L. Uranium concentrations decrease considerably with depth, to about 1 μg/L below 50 m. Fluoride concentrations decrease to a few mg/L at depth and sulphate is in the range of 10–20 mg/L. These concentration changes with depth suggest strongly oxidising conditions and very active circulation of groundwaters in the top 10 metres and then perhaps moderately oxidising conditions combined with active groundwater circulation down to about 50 metres depth. This essentially conforms with the known hydrological pattern.

The shallow waters show significantly high proportions of Fe(III)/Fe(tot) and high uranium concentrations, whereas at or below about 50 m nearly all of the dissolved iron is Fe(II) and the uranium is consistently low. Therefore, the groundwater below 50 m reflects reducing conditions, which is consistent with the hydrogeological data indicating recharge to depths of at least 100 m into unoxidised bedrock containing abundant pyrite. Water then flows with an upward vector as it enters the deep boreholes (see Fig. 2). The depth zone of 10–50 m is an approximate transition region between the near-surface

zone of active circulation and strong oxidation and the deeper zone of chemical reduction and slower flow. The transition region has a rather variable water composition due to two possible effects: the depth variation of the redox front as preserved in the bedrock and the mixing of deep, reduced upward-flowing groundwaters with shallow oxidised groundwaters.

Fluorite is a common gangue mineral and is the only known significant source of fluoride ions. Fluoride is usually about 2–3 times the molal concentration of calcium in the groundwaters, which indicates that most of the fluoride and calcium is coming from fluorite dissolution. Consistently higher concentrations of both calcium and fluoride are seen in the intermediate depth borehole F2 than in the deeper borehole F1. This observation suggests that the groundwaters in the deeper hole see less fluorite along their flow path, which is a well-defined porous zone some 10 m in width, in which any fluorite may already have been leached out. Alternatively, fluorite dissolution rates may be faster at the shallower level for some unknown reason. This observation is also one

TABLE IV

Mass balance and mass transfer results for the F1 borehole (samples PC-GW-42 and the F1 Selected Reference Water Sample) using the programs BALANCE and PHREEQE. Results in mmol/kg of substance dissolved (positive) or precipitated (negative values).

Substance	PC-GW-42		F1	
computed	BALANCE	PHREEQE	BALANCE	PHREEQE
Fluorite	0.0092	0.0092*	0.0108	0.0108*
Calcite	0.0020	0.0020*	0.0009	0.0009*
K-spar	0.330	0.33*	0.325	0.325*
Albite	0.0091	0.0091*	0.0087	0.0087*
Chlorite	0.0007	0.0007*	0.0006	0.0006*
Barite	–	–	0.0009	0.0009*
Kaolinite	–0.1693	–0.1697	–0.1665	–0.1663
Chalcedony	–0.1318	–0.120	–0.0872	–0.1095
Pyrite	0.0814	0.0814*	0.0822	0.0822*
Sphalerite	0.0012	0.0012*	0.0013	0.0013*
Ferrihydrite	–0.0584	–0.0696	–0.0584	–0.0560
MnOOH	0.0033	0.0033*	0.0035	0.0035*
pH	5.25[1]	5.38	4.87[1]	5.30
log P_{CO_2}	–1.777[2]	–1.777[2]	–1.569[2]	–1.569[2]
Eh	+6.80[1]	+6.80[1]	+5.77[1]	+5.77[1]

*These values were taken directly from the BALANCE.

[1]Field measurements.

[2]Computed from pH and alkalinity with WATEQ4F.

of the very few clear differences that can be discerned between the water chemistry in these two boreholes.

Mass balance calculations have been performed using, as for Morro do Ferro, pure water as an input solution. For this area, the F1 sample has been selected as a representative water with a low residence time underground and which is relatively oxidised.

The result from the BALANCE program is shown in Table IV. The same Table reports the reaction path simulation with the PHREEQE program. As before, a constant and relatively high redox potential (Eh$\approx$ +230 mV) has been maintained throughout the simulation. The results show excellent agreement, signifying that the geochemical evolution of these groundwaters can be successfully modelled with the known mineral assemblage, the known water chemistry and the constraints of the thermodynamic data.

7. Conclusions

The application of ion plots and reaction models using speciation, mass balance and thermodynamic mass transfer calculations has provided an excellent model for present-day water/rock interactions at the two sites studied. The dominant processes are:

- Fluorite and calcite dissolution.
- Barite solubility equilibrium.
- K-feldspar and albite dissolution.
- Chlorite (mixed-layer clay) dissolution.
- Kaolinite precipitation.
- Silica precipitation.
- Pyrite and sphalerite oxidation.
- Ferrihydrite precipitation.
- Manganese oxide dissolution.
- High Pco_2 input from soil zone.

These findings are in excellent agreement with the known mineralogy.

8. References

Ball, J.W., Nordstrom, D.K. and Zachmann, D.W., 1987. WATEQ4F – A personal computer FORTRAN translation of the geochemical model WATEQ2 with revised data base. *U.S. Geol. Surv. Open-File Rep.* (87-50), 108 pp.

Ball, J.W., Nordstrom, D.K. and Zachmann, D.W., 1990. Computer code and data base revisions to the personal computer geochemical model WATEQ4F. *U.S. Geol. Surv. Open-File Rep.* (90-). (In press).

Drever, J.I., 1988. The Geochemistry of Natural Waters, 2nd edition, *Prentice-Hall*, 438 pp.

Garrels, R.M., 1967. Genesis of some ground waters from igneous rocks. In: Researches in Geochemistry, Vol. 2, *John Wiley and Sons*, 405-420.

Garrels, R.M. and MacKenzie, F.T., 1967. Origin of the chemical composition of some springs and lakes. *Advances in Chemistry, Series 67. Am. Chem. Soc.*, 222-242.

Millero, F.J., Sotolongo, S. and Izaguirre, M., 1987. The oxidation kinetics of Fe(II) in seawater. *Geochim. Cosmochim. Acta*, 51, 793-801.

Nordstrom, D.K. and Ball, J.W., 1990. Mineral saturation states in natural waters and their sensitivity to thermodynamic and analytical errors. *Sciences Geologiques.* (In press).

Nordstrom, D.K. and Munoz, J.L., 1986. Geochemical Thermodynamics. *Blackwell Sci. Pub.*, 477 pp.

Nordstrom, D.K., Plummer, L.N., Langmuir, D., Busenberg, E., May, H.M., Jones, B.F. and Parkhurst, D.L., 1990. Revised chemical equilibrium data for major water-mineral reactions and their limitations. *Am. Chem. Soc. Symp. Ser. 416*, 398-413.

Parkhurst, D.L., Plummer, L.N. and Thorstenson, D.C., 1982. BALANCE – A computer program for calculating mass transfer for geochemical reactions in ground water. *U.S. Geol. Surv., Water Resour. Invest. Rep.* (82-14), 29 pp.

Parkhurst, D.L., Thorstenson, D.C. and Plummer, L.N., 1980. PHREEQE – a computer program for geochemical calculations, *U.S. Geol. Surv., Water Resour. Invest. Rep.* (80-96; revised 1982 and 1985), 193 pp.

Pearson, F.J., Fisher, D.W. and Plummer, L.N., 1978. Correction of ground-water chemistry and carbon isotopic composition for effects of CO_2 outgassing. *Geochim. Cosmochim. Acta*, 42, 1799-1807.

Plummer, L.N., 1984. Geochemical modeling: A comparison of forward and inverse methods. In: Proceedings First Canadian/American Conference on Hydrogeology. Practical Applications of Ground Water Geochemistry. *National Water Well Assoc.*, 149-177.

Plummer, L.N. and Back, W., 1980. The mass balance approach: application to interpreting the chemical evolution of hydrologic systems. *Am. J. Sci.*, 280, 130-142.

Plummer, L.N., Parkhurst, D.L. and Thorstenson, D.C., 1983. Development of reaction models for ground-water systems. *Geochim. Cosmochim. Acta*, 47, 665-686.

Steyn, J.G.D., 1954. Spectrographic and x-ray data on some fluorites from the Transvaal, South Africa. *Min. Mag.*, 30, 327-332.

Sung, W. and Morgan, J.J., 1980. Kinetics and product of ferrous iron oxygenation in aqueous systems. *Environ. Sci. Technol.*, 14, 561-568.

Theis, T.L. and Singer, P.C., 1974. Complexation of iron(II) by organic matter and its effect on iron(II) oxygenation. *Environ. Sci. Technol.*, 6, 569-573.